https://doi.org/10.5194/essd-2020-83
Preprint. Discussion started: 29 June 2020

Open Access Earth System Science Data Discussions

Constructing a complete landslide inventory dataset for the 2018 Monsoon disaster in Kerala, India, for land use change analysis

Lina Hao[1,2], Rajaneesh A.[3], Cees van Westen[2], Sajinkumar K.S.[3,4], Tapas Ranjan Martha[5], Pankaj Jaiswal[6], Brian McAdoo[7]

[1]State Key Laboratory of Geohazard Prevention and Geoenvironment Protection, Faculty of Earth Sciences, Chengdu University of Technology, Chengdu, China
[2]Faculty of Geoinformation Science and Earth Observation (ITC), University of Twente, Enschede, the Netherlands
[3]Department of Geology, University of Kerala, Thiruvananthapuram 695581, Kerala, India
[4]Department of Geological & Mining Engineering & Sciences, Michigan Technological University, USA
[5]National Remote Sensing Centre, Indian Space Research Organisation, Hyderabad, India
[6]Geological Survey of India (GSI)
[7]Yale-NUS College, Singapore

Correspondence to: Lina Hao (hao_ln@qq.com) and Cees van Westen (c.j.vanwesten@utwente.nl)

Abstract. Event-based landslide inventories are important for analyzing the relationship between the intensity of the trigger (e.g. rainfall, earthquake) and the density of the landslides in a particular area, as a basis for the estimation of the landslide probability and the conversion of susceptibility maps into hazard maps required for risk assessment. They are also crucial for the establishment of local rainfall thresholds that are the basis of Early Warning Systems, and for evaluating which land use / land cover changes are related to landslide occurrence. The completeness and accuracy of event-based landslide inventories are crucial aspects to derive at reliable results or the above types of analysis. In this study we generated a relatively complete landslide inventory for the 2018 Monsoon landslide event in the state of Kerala, India, based on two inventories that were generated using different methods: one based on Object Based Image Analysis (OBIA) and the other on field surveys of damaging landslides. We used a collaborative mapping approach based on the visual interpretation of pre-and post-event high-resolution satellite images available in Google Earth, adjusted the two inventories and digitize landslides that were missed in the two inventories. The reconstructed landslide inventory database contains 4728 landslides consisting of 2477 landslides mapped by OBIA method, 973 landslides mapped by field survey, 422 landslides mapped both by OBIA and field method and an additional 856 landslides mapped using the visual image (GE) interpretation. The dataset is available at https://doi.org/10.17026/dans-x6c-y7x2 (van Westen, 2020). Also, the location of the landslides was adjusted, based on the image interpretation, and the initiation points were used to evaluate the land use/land cover changes as a causal factor for the 2018 Monsoon landslides. A total of 45 % of the landslides that damaged buildings occurred due to cut-slope failure while 34% of those impacting on roads were due to road cut-slope failures. The resulting landslide inventory is made available for further studies.

https://doi.org/10.5194/essd-2020-83
Preprint. Discussion started: 29 June 2020

Open Access Earth System Science Data Discussions

1 Introduction

Landslides are a significant type of natural hazard, occurring worldwide and incurring serious losses to human society. Landslide frequently damage buildings, communication systems, agriculture, natural vegetation, environment and are a major cause of fatalities (Froude and Petley, 2018; Petley et al., 2005). A landslide inventory forms the basis for studies of landslide hazard, risk and prevention studies (Fan et al., 2019; Guzzetti et al., 2012; Marcelino et al., 2009; Moosavi et al., 2014). Critical elements of analysis include their spatial distribution pattern (Duman et al., 2005; Galli et al., 2008; Xu, 2015), their occurrences with respect to landform evolution (Guzzetti et al., 2012; Rosi et al., 2018) and a range other environment factors (Duman et al., 2005), susceptibility mapping (van Den Eeckhaut et al., 2009), triggering factors (Li et al., 2016), community risk assessment and mitigation (Marcelino et al., 2009), and land use planning and risk management (Colombo et al., 2005). A detailed landslide inventory should contain information on location, types of failures, geometries, date of occurrence, triggering factors, possible failure mechanisms, and damage caused (Rosi et al., 2018). Landslide inventory maps can be generated by compiling existing historical landslide data or acquiring new landslide data using a variety of technical approaches (Rosi et al., 2018; Santangelo et al., 2015).

A new landslide inventory that is generated after a major triggering event, e.g. an earthquake, storm, snowmelt and volcanic eruptions, is referred to as an event-based landslide inventory (Fiorucci et al., 2011; Galli et al., 2008; Rosi et al., 2018). Methods for event-based landslide inventories include field investigation, visual interpretation, and often an automatic image classification. Field investigation shortly after the event (Fiorucci et al., 2011; Mondini et al., 2011) allows for the collection of detailed information through field surveys recording information on the location, types, volumes, contributing factors, and damages (Yang and Chen, 2010). Visual interpretation based on remote sensing images (Alkevli and Ercanoglu, 2011; Mondini et al., 2011; Samodra et al., 2018), allows to map and classify landslides in terrain that is less accessible. This method will be more accurate with higher-resolution of the available before and after event images (Li et al., 2013; Xu et al., 2013; Zhong et al., 2019). Automated classification of remote sensing images is a means to rapidly map many landslides over large areas, using different classification algorithms (Lei et al., 2018; Plank et al., 2016; Yang and Chen, 2010), such as supervised classification (Lacroix et al., 2013), Object Based Image Analysis (OBIA)(Behling et al., 2014; Casagli et al., 2016; Keyport et al., 2018; Lahousse et al., 2011; Mohan Vamsee et al., 2018), Markov random fields (Lu et al., 2019; Qin et al., 2018), random forests (Stumpf and Kerle, 2011), support vector and other machine learning methods (Lei et al., 2019) or a combination of various algorithms (Aksoy and Ercanoglu, 2012; Li et al., 2016; Lu et al., 2011; Stumpf and Kerle, 2011). With the continuous improvement of earth observation technology, such as UAV, high-resolution optical satellite remote sensing, SAR, InSAR, it is more feasible to acquire remote sensing images before and after an event, which lead to more landslide inventory maps (Casagli et al., 2016; Santangelo et al., 2015; Solari et al., 2019; Travelletti et al., 2012). Often the field surveys method are combined with remote sensing based methods to improve veracity (Ardizzone et al., 2012; Galli et al., 2008; Mondini et al., 2011; Oh and Pradhan, 2011; Rosi et al., 2018; Trigila et al., 2010).

Between 1 June and 26 August 2018, the southern Indian state of Kerala witnessed the most severe extreme rainfall event

https://doi.org/10.5194/essd-2020-83
Preprint. Discussion started: 29 June 2020

since 1924 (Agarwal, 2018; Megha et al., 2019; Sankar, 2018; Vishnu et al., 2019). The torrential rains triggered several thousand landslides (Singh et al., 2018), and extensive flooding, affecting 5.4 million people in over 1,200 villages, causing enormous property losses (buildings, roads and agriculture damages) and more than 440 casualties (Mishra et al., 2018; Vishnu et al., 2019). Furthermore, the following year, from August 8-14, 2019, Kerala was hit again by another extreme precipitation event, causing more than 100 deaths due to landslides and floods (NDTV, 2019). Due to these severe events, both the United Nations Environment Programme (UNEP) and the Government of Kerala came together to study the causes of the extreme occurrences of slope failure in this region. Concern was raised whether anthropogenic activities such as deforestation and agriculture exacerbate the occurrence of mass movements in this region. In order to study this, a complete event-based landslide inventory is necessary to combine with detailed land use information to determine a causal relationship.

In this research, we generated a complete landslide inventory for the 2018 Monsoon event in Kerala, using a collaborative mapping approach based on the visual interpretation of pre-and post-event high-resolution satellite images available in Google Earth, and two pre-existing inventories. This manuscript focuses on the generation of the dataset consisting of a detailed landslide inventory with respect to available land use information. The ultimate aim of the study is to have a comprehensive database that can be used to analyze to what extent the 2018 landslides were affected by land use changes.

2 Study area and data sources

2.1 Study area

Kerala is one of the most susceptible areas to mass movements in India (Sreekumar, 2009; Vasudevan and Ramanathan, 2016), with a long history for the natural occurrence of slope instability going back to 1341 AD (Kuriakose et al., 2009). Both climate and landform of Kerala are conducive to slope failures. Kerala is located in the southwest of India Peninsula, in the windward slope of the Western Ghats (Sajinkumar et al., 2011), on the east coast of the Arabian Sea (Figure 1a), this determines Kerala's typical tropical climate (the average minimum and maximum temperatures are 22 ℃ and 34 ℃) with two monsoon seasons. The southwest monsoon, lasting from June to September, delivers 80% of the annual rainfall (Paul et al., 2016), and the remainder falls in the northeast monsoon lasting from October to November. The annual average rainfall in this area is 200 to 500cm, which increases from the southwestern coastal plains to the mountain areas in the east due to the orographic effect of the Western Ghats (Kuriakose et al., 2009; Sajinkumar et al., 2011). Under the global climate change, extreme rainfall events have hit India frequently (Mishra et al., 2018) and the extreme rainfall events during the monsoon season are expected to increase (Hunt and Menon, 2020; Rai et al., 2019, 2020; Shashikanth et al., 2018), making it more vulnerable to slope failures.

Owing to the tropical climate, the bedrock weathering is strong in Kerala, leading to most of this area being covered with thick poorly consolidated soil (Sajinkumar et al., 2011). The main soil is laterite with average thickness of 5m depending on the slope (Kuriakose et al., 2009). Physiographically, Kerala can be divided into two units- a plateau with rugged mountains

https://doi.org/10.5194/essd-2020-83
Preprint. Discussion started: 29 June 2020

and deep valleys in the east and coast plains in the west (Figure 1b) (Kuriakose et al., 2009; Sajinkumar and Anbazhagan, 2015; Vishnu et al., 2019). The Western Ghats are controlled by ancient faulted escarpments located along the plateau, often with very steep slopes, which are susceptible to slope failures (Kuriakose et al., 2009). Metamorphic rocks, such as Charnockites, Khondalites and Gneisses are the predominant rock types in Kerala (Kuriakose et al., 2009; Sajinkumar and Anbazhagan, 2015). The combination of highly weathered bedrock and steep slopes in a monsoon climate make each district in Kerala (save the whole coastal plain district-Alappuzha) susceptible to slope instability (Figure 1) (Kuriakose et al., 2009; Sajinkumar and Anbazhagan, 2015)

2.2 Original Data

Two landslide inventories for the 2018 triggering rainfall event were available. The first inventory came from the National Remote Sensing Center (NRSC), of the Indian Space Research Organization (ISRO) who did a rapid mapping project aimed to quickly identify slope failures in the whole Western Ghats region. They used a combination of visual image interpretation and semi-automated landslide detection based on OBIA algorithm (Martha et al., 2010, 2011, 2012, 2013, 2016). They used multi-temporal images acquired before and after the monsoon rainfall event from Resourcesat-2 and Sentinel-2 Earth observation satellites (Martha et al., 2019), resulting in an inventory with 5191 landslide polygons for Kerala (Martha et al., 2019). This rapid assessment was crucial for the emergency response by the disaster management authorities in Kerala. The fast mapping method allowed to determine the general distribution, density and size of landslides in order to plan for the relief operations and overall assessment. In this study, the original NRSC data was obtained as polygon shape-file (Figure 2), and then the shape-file was converted into KML for the following visual interpretation.

Another landslide inventory was generated by the Geological Survey of India (GSI) in collaboration with the Kerala State Disaster Management Authority (KSDMA), with the aim to make a detailed survey of the landslides that specifically caused damage to buildings, roads and other infrastructure. It is important to recognize this deliberate bias in the dataset, as almost all landslides would have been mapped near roads, and is almost by definition going to be related to human occupation and transformation of the land. During a period of several months after the event, teams from GSI visited hundreds of sites with landslide damage. The landslides characteristics were recorded in data sheets, and transferred to spreadsheets with many attributes, including *the names of administrative units, latitude, longitude, types of slide, buildings affected, road affected, recommendations, and remarks*. The GSI landslide data spanned for 10 districts (Figure 2), and the landslides studied were mainly along roads. A total of 1437 landslides points were converted into a point shape-file with all the attributes using ArcGIS 10.3, and KML for easier visual interpretation in Google Earth.

3 Methodology

After combining the above-mentioned inventories and overlaying them on high-resolution satellite images from before and after the event in Google Earth, several issues with the data were discovered through visual interpretation. The issues from

https://doi.org/10.5194/essd-2020-83
Preprint. Discussion started: 29 June 2020


Open Access Earth System Science Data Discussions

the NRSC inventory included (a) some landslides had no noticeable changes visible on the high-resolution images from before and after the event, therefore these were excluded from the inventory (Figure 3a, 3b), (b) there were changes on images before and after the event, however the changes were not caused by landslide, but by other factors, i.e. vegetation clearing (Figure 4a, 4b, 4c) or engineering activities (Figure 4d, 4e, 4f), and these were also excluded from the inventory, (c) the location of landslide polygons mismatched positionally with the landslide scarps visible in the images (Figure 5b, Figure 6b), as the NRSC data was mainly based on Resourcesat-2 LISS IV images with 5.8 m spatial resolution, (d) large landslides in the inventory were sometimes mapped as several smaller ones (Figure 5b), and in contrast small landslides were sometimes included in larger ones (Figure 6b).

Also the landslide points of the GSI inventory had some issues, namely (a) that the surveyors also marked some points where cracks or small subsidence had occurred, that did not lead to an actual landslide, (b) some of the landslide points could not be recognized as slope failures in the images, if they were too small to be recognized or sheltered by shadows, trees or buildings (Figure 7a, 7b), and (c) the location of the landslide point did not match with a visible landslide scarp on the image (Figure 8b).

Problems were also found with the use of the Google Earth images, and landslides clearly identified in the NRSC inventory could not be visually confirmed due to (a) a large time gap between the 2018 Monsoon and the first available image after the event, which caused problems with identification in Google Earth images due to the fast re-growth of vegetation (Figure 9b), (b) the poor quality of the post-event images in Google Earth, due to distortion induced by steep slopes (Figure 10b, 10c), shadows induced by steep slopes (Figure 11b), clouds obstructing the view (Figure 12b), and (c) the limited geographic coverage of post-event images, which prevented the verification of the other datasets.

As these issues of veracity were quite important, and would affect the analysis of land use changes substantially, we decided to correct and edit all landslides using visual interpretation based on multi-temporal high-resolution images available before and after the event on the Google Earth platform, and using additional Resourcesat-2 LISS-IV images, with a spatial resolution of 5.8 m from NRSC for those locations where post-event satellite images in Google Earth were distorted, obscured or missing. By using two screens, the same landslide area was visualized using Google Earth on one screen (with KML files of the landslide points or polygons) and ArcGIS on another screen with shape files. With the aid of the historical image viewer tool from Google Earth, the landslides were evaluated, interpreted, assessed and measured on one screen by experts comparing multi-temporal images for the same area, while edited on the other screen for the same area. Our final landslide inventory dataset was made as points, which were carefully located on the initiation point of the landslides, as our aim was to correlate these with land use / land cover changes. The workflow for the landslide inventory is shown in Figure 13.

3.1 Landslide mapping

The landslide mapping included the correction of the available polygons (from NRSC) and points (from GSI), and adding new landslides that were overlooked by the available existing inventories. For the polygons from NRSC, the correction

https://doi.org/10.5194/essd-2020-83
Preprint. Discussion started: 29 June 2020


Open Access Earth System Science Data Discussions

included (a) removing false positive polygons (Figure 3 and Figure 4), (b) digitizing a landslide point at the top of the landslide scarp where the actual landslide is inside or close to the polygon (Figure 5c, Figure 6c), and (c) for areas with NRSC landslide polygons but where post-event images in Google Earth were of poor quality or missing, a landslide point was digitized at the top of the landslide scarp based on available Resourcesat-2 LISS IV, and Sentinel-2 images by overlapping the same polygon to both image available at NRSC and Google Earth, and comparing it with the Google Earth 3D terrain. As all the landslide points from GSI were mapped in the field by geologists, we (a) only removed those points which were not classified as actual landslides but as zones with cracks and subsidence, (b) retained all the other points and their locations even when the landslide scarps could not be recognized on images (Figure 7a, 7b), and (c) where the GSI landslide location did not match the image, we moved the landslide point to the scarp (Figure 8c). Using this procedure, the entire area was carefully checked through visual comparison of images before and after the event, and landslides that were missed in the two available inventories were added by digitizing a point on the top of their scarp.

Due to the existing attributes recorded in the GSI inventory and our project aim of analysis relation between LULC and landslides, attributes that were considered important were edited, including failures type, length, width, area, damages to building, road and agriculture, specific reasons for failure, and the land use in 2010 and 2018. Considering the limited ability of identifying landslide diagnostic features from multi-temporal high-resolution images in Google Earth and failures types recorded in GIS inventory, the landslides were classified into three simple groups: surficial slide (SS), debris flows (DF) and rock fall (RF). The length and width attributes represent the maximum length and width of the landslide, which were measured either in Google Earth or in ArcGIS. Based on the GSI survey data and our interpretation of the satellite data we marked those landslides which caused damage to buildings, to roads, and to agricultural land. Wherever possible we identified the apparent reasons for failure on images such as (1) building cutslope failure, (2) road cutslope failure, (3) inadequate drainage along the road, (4) reactive of old landslides, (5) undercutting of slope by river, (6) reservoir increase causing instability along slopes, (7) deforestation, (8) clearing of tea plantation, (9) clearing of rubber plantation, (10) the margin area between different land use types.

3.2 Land use attributes

In order to study the relation between landslides and recent land use changes, detailed and precise land use information immediately before the 2018 event was required, together with land use information for some time earlier. The available online land cover products, such as IGBP DISCover, UMD Land Cover, Global Land Cover 2000 and GlobCover 2009 (Congalton et al., 2014), have too coarse resolution for a proper correlation with the landslides (Seo et al., 2014). Several historical digital land use maps from Kerala were also available from the Kerala State Disaster Management Agency (KSDMA), however, after careful comparison with the corresponding high-resolution images using Google Earth history viewer, we decided not to use them because of the insufficient spatial and thematic accuracy. Figure 14a illustrates this by overlaying the 2010 land use map on the high-resolution satellite images of the same year. The first problem is that the land use polygons do not match the image information (i.e. the shape of polygon A and B do not match with the image from the

https://doi.org/10.5194/essd-2020-83
Preprint. Discussion started: 29 June 2020


Open Access Earth System Science Data Discussions

same year). The second problem is that the land use polygons in this 1:50.000 scale land use map are too generalized for analyzing specific relations with landslides. One land use polygon may contain more than one land use type, i.e. the land use type of polygon B is *Tea*, while on the detailed images it can been interpreted that it contains roads, buildings, shrubs, bare farm land, and forest as well (Figure 14a). If this map was used for correlating landslide occurrences with land use types, the land use type in 2010 of all landslides in Figure 14b would have been *Tea*. However, the actual land use types were bare farmland (landslide I, III and IV) and shrub plantation (landslide II and V) (Figure 14c). In order to correlate landslide occurrences with the land use (change) at specific locations (like landslide scarps), detailed and accurate land use data are needed. Automatic image classification would not give the required accuracy and detail (Srivastava et al., 2012), due to the complexity of the terrain and the detailed land use legend needed. It has proven very difficult to differentiate natural land use types (e.g. forest) from cultivated area (e.g. mixed forest plantations) using automatic image classification. Automatic image classification also requires a large number of very high resolution cloud free images for at least two periods covering the whole landslide affected area of Kerala, which require costs that were beyond the scope of this project.

In view of the above problems, we decided to visually interpret the land use types for each landslide based on the Google Earth history viewer, in which the oldest and nearly complete cover of high-resolution images for Kerala dates back to 2010. Visual interpretation is useful in land use mapping (Butt et al., 2015; Mohammady et al., 2015; Kibret et al., 2016) with higher accuracy (Audah et al., 2019; Ghorbani and Pakravan, 2012) especially in complicated areas (Huang et al., 2018). A skilled interpreter, who is familiar with land use types and was trained to identify diagnostic features of various land use types in the study area, is able to extract detailed land use information from the image interpretation elements of pattern, shape, context, size, shadows, phenology, spatial relation, and changes (Cihlar and Jansen, 2001), as well as using clues from available land use maps from NRSC for differentiating cultivation from natural vegetation. Differentiating agriculture from natural vegetation was considered important to model relationship between landslides and land use. An interpreter will be generally be able to discriminate the boundaries of complicated land use types with a higher accuracy than can be obtained through automatic classification, although it will take much more time (Miettinen et al., 2019). The use of Google Earth history viewer allows to frequently compare the temporal image characteristics of the same area using vertical as well as oblique views in different directions, which are all helpful in recognizing land use types. Furthermore, the land use in the direct surrounding of the landslide can be interpreted as well, allowing the interpreters to make a better evaluation of the relation between land use and landslides. For each landslide the land use situation was evaluated for the year 2010 and for the year 2018, prior to the occurrence of the extreme event in August 2018. The mapping was done as a collaborative mapping exercise, involving a group of four mappers. A detailed legend was worked out first and discussed among the mappers, in order to achieve a standard interpretation. Also, regular cross-checks were made of each other's results to ensure a standardized approach. The ability to visually differentiate land use types was taken into account in defining the land use legends (Fox et al., 2017). Land use /land cover types were selected in such a way that they differed with respect to their influence on landslides, in terms of vegetation cover, anthropogenic activities, hydrological effects and root characteristics (Karsli et al., 2009; Reichenbach et al., 2014). Ultimately, twenty five land use types were defined in our study (see Figure

https://doi.org/10.5194/essd-2020-83
Preprint. Discussion started: 29 June 2020

16). For each landslide point on the top of a landslide scarp, the historical image viewer of Google Earth was used to visualize the surrounding areas before failure in 2018 using the earliest available images, and the land use situation around 2010 (using the image that is closed to this date).

4 Resulting landslide inventory

4.1 Complete Landslide inventory for the 2018 Kerala Monsoon event

After the landslide mapping and attribute editing, a complete landslide point inventory dataset for the 2018 Monsoon event in Kerala was generated, containing 4728 confirmed landslides. Out of these, 2477 landslides (52%) were derived from the NRSC polygons, and 973 landslides (21%) from the GSI points with, 422 landslides (9%) that were included in both inventories. Additionally, 856 new landslide points (18%) were digitized (Table 1, Figure 15a). The most common landslide type was *debris flow* (DF: 2816 landslides), followed by *surficial slide* (SS: 1760) and *rock fall* (RF: 152) (Table 2, Figure 15b). The landslide types for the NRSC inventory were interpreted by us using the visual mapping of the Google Earth images. They differed from the GSI landslide inventorys, with a higher proportion of debris flows in the NRSC data (71% of the polygons were DF, 25% SS and 4% RF) as compared to the GSI data (44% DF, 55% SS and only 1% RF). The Idukki district was mostly affected by landslides, accounting for 47.02% of the total landslides in Kerala (Figure 15).

Figure 16 shows the frequency of landslides for the different land use/land cover types in 2010 and 2018. The results show that the highest proportion of the landslides were initiated in Mixed Plantation Forests (FMP, 25.06%), followed by Dense Natural Forests (FDN, 23.33%). This is an interesting result in view of the expectation that forests are less vulnerable to landslides, due to the hydrological and geomechanical characteristics of trees which tend to reduce the chance of slope stability (Alcántara-Ayala et al., 2006; Reichenbach et al., 2014; Tasser et al., 2003). Also a significant percentage of 14% of all landslides occurred in steep areas with bare rock and soil and sparse vegetation.

Among all the landslides in this event in Kerala, 2503 out of 4728 landslide caused damages to buildings, roads and agricultures, accounting for 52.94%. Apart from the 1205 damaging landslides surveyed in the field by GSI, the image interpretation revealed another 90 landslides with damage to buildings, 356 with damage to roads, and 1251 with damage to agriculture (Figure 17). As for building impacts, 645 landslides destroyed 942 buildings, of which most were residential buildings (Figure 17). A surficial slide (SS) in Kannur damaged 23 buildings while a debris flow (DF) in Wayanad destroyed 12. Landslides associated with building cut-slopes were responsible for 45% of the damaged buildings. Regarding road impacts, 897 landslides caused traffic disruption after the event, among which 625 landslides covered roads which need to be cleared while 272 landslides damaged roads that had to be repaired. Landslides associated with road cut-slopes were responsible for 34% of the road impacts. For agriculture impacts, 2194 landslides destroyed the agricultural land use classes of TEA, FMP, RUB, SPL and FCP (Figure 16). FMP, SPL and TEA suffered the most damages of all cultivation land.

The results show that only a relatively small number of landslides (707, 14.95%) were located in sites where land use changes occurred in the past eight years before their occurrence (Figure 16). The vast majority of the landslides were not

https://doi.org/10.5194/essd-2020-83
Preprint. Discussion started: 29 June 2020

related to land use changes in the past decade.

4.2 Comparison of inventories

The final landslide dataset was made by integrating two inventories that were acquired using different methods. In the final inventory, 2899 (61.32%) out of 4728 landslides were obtained directly from the results of the automatic classification, which were accepted after careful visual interpretation of multi-temporal high-resolution remote sensing images. Among the 2899 landslides, 2657 landslides were mapped as points directly from an equal number of polygons, 163 landslide points were made by merging 366 polygons (when several polygons belonged to the same landslide), and 79 landslides were mapped by separating 35 polygons (when a single polygon contained several landslides). Only 422 out of 1437 landslides with confirmed damage, mapped by GSI, were identified by automatic image classification.

5 Data availability

The landslide dataset, and a document with metadata, is freely downloadable from https://doi.org/10.17026/dans-x6c-y7x2 (van Westen, 2020) and available for further analysis. The landslide dataset is provided in the form of an ESRI point shape-file including the following attributes: *district*, *landslide type*, *area*, *damage* (building impact, road impact, and agriculture impact), *land use in 2010*, *land use in 2018*, *specific reasons for landslide occurrence*, *remarks* and *data source*. The definition of each attribute and the codes are provided in an accompanying metadata Word document. The dataset aims to contribute to further understanding of the relation between rainfall intensities and associated spatial distribution of landslides, in order to improve the methods for rainfall-induced landslide hazard assessment, and the development of more accurate rainfall thresholds for early warning. The dataset also aims to contribute to further research on the relation between land use changes and landslide occurrences, which is also an important aspect, especially due to the observed increase in extreme hydro-meteorological hazard events.

6 Discussion and conclusions

The results show that more than half of the damaging landslides (613) surveyed by GSI, were very small (<500 m^2). Many of these small-sized landslides could not be visually identified and measured even on high-resolution images, for they may be covered by dense vegetation or sheltered by buildings and other objects. This makes it also very difficult to detect them using automatic image classification, as no more than half of these damaging landslides (422 out of 973) were detected. This is an important factor as the automatic image classification provides a rapid survey of the possible landslide area, soon after the event. Reconnaissance in the field by geologists is the best method for mapping such landslides (Brardinoni et al., 2003). The survey requires considerably more time and resources, and it took survey teams of 20 persons one month to carry out the survey, with a follow up survey by 10 persons for another three months. The survey was also biased towards damage along

https://doi.org/10.5194/essd-2020-83
Preprint. Discussion started: 29 June 2020

the roads. Although time consuming and biased toward to landslides close to road, field-based surveys remain an essential component for the damage assessment and post-disaster recovery as it will obtain quantitative information on the damage caused by landslides and will neither be replaced by image interpretation nor automatic image classification (Moosavi et al., 2014).

For landslides with an area larger than 1000 m^2, automatic image classification is a very useful tool, as evidenced by this study, where more than 76.3% of all large landslides were detected automatically. The automatic classification method is useful for detecting landslide with a certain minimum size (Lahousse et al., 2011; Martha et al., 2011) depending on the resolution of remote sensing images (Fiorucci et al., 2011; Harp et al., 2011). OBIA is very effective for generating a rapid first inventory of larger landslides triggered by an event such as intense rainfall and earthquake (Behling et al., 2014; Lu et al., 2011; Martha et al., 2016). However, the accuracy of these automatic recognition methods still need to be improved (Feizizadeh et al., 2017), and care should be taken to derive statistical relationships with causal factors from such inventories due to the significant overestimation of the number of landslides, and because the relations would only be meaningful for the initiation areas of the landslides, and not for the full polygon areas that are normally identified using OBIA.

During this Monsoon event triggered landslide inventory, it took teams of 6 persons 39 days (one person works 8 hours per day) for the visual interpretation checking and digitizing. Comparing automatic image classification, visual interpretation of satellite data is a cost-effective, yet quite time consuming method for mapping event-triggered landslides (Yu and Chen, 2017), and has a high accuracy if combined with field investigation (Fiorucci et al., 2011; Mondini et al., 2011). Also, landslides above a minimum size of 20 m^2 can be recognized based on sub-meter high-resolution images, if they are not masked by shadows of nearby slopes, objects or vegetation. The comparison of pre-and post-event satellite images, and the integration with the results of automatic image classification in a platform such as Google Earth history viewer, was very useful for the generation of a complete and reliable inventory. The collaborative mapping approach, involving a number of mappers, in different locations, required a good communication and cross-checking of the interpretation results, to ensure consistent results among the mapper, but reduced the mapping time comparing to field-based survey method, and the costs for image acquisition were greatly reduced by using Google Earth images (van Westen et al., 2008).

The Monsoon event of 2018 in Kerala triggered 4728 landslides, which damaged 942 buildings, and killed 483 persons (Sahana, 2019). It was an extreme event, and the damage was attributed in popular literature to climate change and anthropogenic changes, especially the decrease of natural forests and the increase of buildings in sloping terrain (The Conversation, 2019). Recent studies (Ramachandra and Bharath, 2019) have analysed that the forest cover in the Western Ghats has decreased by 30%, from 16.21% in 1985, to 11.3% in 2018. The region now has 17.92% plantation area, 37.53% agriculture and 4.88 % mining and built-up urban areas. It is therefore remarkable that the majority of the landslides triggered during the 2018 monsoon event occurred within forested areas. Also for the vast majority of the landslides no significant changes in land use were detected in the past 8 years, suggesting that this was indeed an extraordinary rainfall event where land use played a relatively minor role. Further research is needed to study the intricate relations between land use change and landslide occurrence.

https://doi.org/10.5194/essd-2020-83
Preprint. Discussion started: 29 June 2020

So far, the final inventory of significant landslides those that damaged buildings, roads, or agricultural areas as well as failures large enough to be seen in various satellite images, can be considered relatively complete for the 2018 event, as the entire area was carefully checked using multi-temporal visual image interpretation. However, it is possible that a few landslides were still missed in the final dataset due to the very small size and shelter. It is not possible to quantify the completeness of the final inventory, due to the lack of another independent and confirmed complete inventory.

Author contributions

LH, CW designed the work together with SKS. LH and RA compiled the dataset. LH wrote the manuscript supervised by CW. TRM and PJ provided some of the data, and suggestions on some methods. LH, RA and SKS performed the figures. CW and BMA provided suggestions on structure, methods and figures. All the authors contributed to the review of the manuscript and approved the dataset.

Competing interests

The authors declare that they have no conflicts of interest.

Acknowledgements

We thank the United Nations Environmental Programme (UNEP) (Muralee Thummarukudy, Karen Sudmeier-Rieux, and Louise Schreyers) for initiating this work and the coordination; Sekhar Lukose Kuriakose and colleagues from the Kerala State Disaster Management Agency (KSDMA) for their support; the National Remote Sensing Centre (NRSC) for providing the landslide polygon inventory; the Geological Survey of India (GSI) for providing the landslide point inventory; and Google Earth for the use of multi-temporal high-resolution remote sensing images. The research was also co-funded by UNEP and the Chinese National Science Fund (grant no. 41702358, 41790445, 41630640, 41771444) and the China Postdoctoral Science Foundation (grant no. 2017M622982).

References

Agarwal, R.: Original Research Article Lesson Learned from Killer Floods in Kerala : Time for Retrospection, Manag. Econ. Res. J., 4, 268–280, 2018.

Aksoy, B. and Ercanoglu, M.: Landslide identification and classification by object-based image analysis and fuzzy logic: An example from the Azdavay region (Kastamonu, Turkey), Comput. Geosci., 38(1), 87–98, doi:10.1016/j.cageo.2011.05.010, 2012.

https://doi.org/10.5194/essd-2020-83
Preprint. Discussion started: 29 June 2020

Alcántara-Ayala, I., Esteban-Chávez, O. and Parrot, J. F.: Landsliding related to land-cover change: A diachronic analysis of hillslope instability distribution in the Sierra Norte, Puebla, Mexico, Catena, 65(2), 152–165, doi:10.1016/j.catena.2005.11.006, 2006.

Alkevli, T. and Ercanoglu, M.: Assessment of ASTER satellite images in landslide inventory mapping: Yenice-Gökçebey (Western Black Sea Region, Turkey), Bull. Eng. Geol. Environ., 70(4), 607–617, doi:10.1007/s10064-011-0353-z, 2011.

Ardizzone, F., Basile, G., Cardinali, M., Casagli, N., Del Conte, S., Del Ventisette, C., Fiorucci, F., Garfagnoli, F., Gigli, G., Guzzetti, F., Iovine, G., Mondini, A. C., Moretti, S., Panebianco, M., Raspini, F., Reichenbach, P., Rossi, M., Tanteri, L. and Terranova, O.: Landslide inventory map for the Briga and the Giampilieri catchments, NE Sicily, Italy, J. Maps, 8(2), 176–180, doi:10.1080/17445647.2012.694271, 2012.

Audah, S., Nazliyati, N., Bakruddin, B., Saputra, E., Wathan, S. and Rizky, M. M.: Visual Analysis of Satellite Landsat Images Multitemporal and GPS as a Geographic Information System for Mapping of Nugmet Plantations in Tapaktuan, IOP Conf. Ser. Mater. Sci. Eng., 506(1), doi:10.1088/1757-899X/506/1/012037, 2019.

Behling, R., Roessner, S., Kaufmann, H. and Kleinschmit, B.: Automated spatiotemporal landslide mapping over large areas using rapideye time series data, Remote Sens., 6(9), 8026–8055, doi:10.3390/rs6098026, 2014.

Brardinoni, F., Slaymaker, O. and Hassan, M. A.: Landslide inventory in a rugged forested watershed: A comparison between air-photo and field survey data, Geomorphology, 54(3–4), 179–196, doi:10.1016/S0169-555X(02)00355-0, 2003.

Butt, A., Shabbir, R., Ahmad, S. S. and Aziz, N.: Land use change mapping and analysis using Remote Sensing and GIS: A case study of Simly watershed, Islamabad, Pakistan, Egypt. J. Remote Sens. Sp. Sci., 18(2), 251–259, doi:10.1016/j.ejrs.2015.07.003, 2015.

Casagli, N., Cigna, F., Bianchini, S., Hölbling, D., Füreder, P., Righini, G., Del Conte, S., Friedl, B., Schneiderbauer, S., Iasio, C., Vlcko, J., Greif, V., Proske, H., Granica, K., Falco, S., Lozzi, S., Mora, O., Arnaud, A., Novali, F. and Bianchi, M.: Landslide mapping and monitoring by using radar and optical remote sensing: Examples from the EC-FP7 project SAFER, Remote Sens. Appl. Soc. Environ., 4, 92–108, doi:10.1016/j.rsase.2016.07.001, 2016.

Cihlar, J. and Jansen, L. J. M.: From Land Cover to Land Use: A Methodology for Efficient Land Use Mapping over Large Areas, Prof. Geogr., 53(2), 275–289, doi:10.1111/0033-0124.00285, 2001.

Colombo, A., Lanteri, L., Ramasco, M. and Troisi, C.: Systematic GIS-based landslide inventory as the first step for effective landslide-hazard management, Landslides, 2(4), 291–301, doi:10.1007/s10346-005-0025-9, 2005.

Congalton, R. G., Gu, J., Yadav, K., Thenkabail, P. and Ozdogan, M.: Global land cover mapping: A review and uncertainty analysis, Remote Sens., 6(12), 12070–12093, doi:10.3390/rs61212070, 2014.

Duman, T. Y., Çan, T., Emre, Ö., Keçer, M., Doğan, A., Ateş, Ş. and Durmaz, S.: Landslide inventory of northwestern Anatolia, Turkey, Eng. Geol., 77(1–2), 99–114, doi:10.1016/j.enggeo.2004.08.005, 2005.

Van Den Eeckhaut, M., Reichenbach, P., Guzzetti, F., Rossi, M. and Poesen, J.: Combined landslide inventory and susceptibility assessment based on different mapping units: An example from the Flemish Ardennes, Belgium, Nat. Hazards Earth Syst. Sci., 9(2), 507–521, doi:10.5194/nhess-9-507-2009, 2009.

https://doi.org/10.5194/essd-2020-83
Preprint. Discussion started: 29 June 2020

Fan, X., Scaringi, G., Domènech, G., Yang, F., Guo, X., Dai, L., He, C., Xu, Q. and Huang, R.: Two multi-temporal datasets that track the enhanced landsliding after the 2008 Wenchuan earthquake, Earth Syst. Sci. Data, 11(1), 35–55, doi:10.5194/essd-11-35-2019, 2019.

Feizizadeh, B., Blaschke, T., Tiede, D. and Moghaddam, M. H. R.: Evaluating fuzzy operators of an object-based image analysis for detecting landslides and their changes, Geomorphology, 293(August 2016), 240–254, doi:10.1016/j.geomorph.2017.06.002, 2017.

Fiorucci, F., Cardinali, M., Carlà, R., Rossi, M., Mondini, A. C., Santurri, L., Ardizzone, F. and Guzzetti, F.: Seasonal landslide mapping and estimation of landslide mobilization rates using aerial and satellite images, Geomorphology, 129(1–2), 59–70, doi:10.1016/j.geomorph.2011.01.013, 2011.

Fox, T. A., Rhemtulla, J. M., Ramankutty, N., Lesk, C., Coyle, T. and Kunhamu, T. K.: Agricultural land-use change in Kerala, India: Perspectives from above and below the canopy, Agric. Ecosyst. Environ., 245(April), 1–10, doi:10.1016/j.agee.2017.05.002, 2017.

Froude, M. J. and Petley, D. N.: Global fatal landslide occurrence from 2004 to 2016, Nat. Hazards Earth Syst. Sci., 18(8), 2161–2181, doi:10.5194/nhess-18-2161-2018, 2018.

Galli, M., Ardizzone, F., Cardinali, M., Guzzetti, F. and Reichenbach, P.: Comparing landslide inventory maps, Geomorphology, 94(3–4), 268–289, doi:10.1016/j.geomorph.2006.09.023, 2008.

Ghorbani, A. and Pakravan, M.: Land use mapping using visual and digital interpretation of tm and google earth images in Shirvandarasi Watershed (north-west of Iran), 33rd Asian Conf. Remote Sens. 2012, ACRS 2012, 2(1), 1823–1828, 2012.

Guzzetti, F., Mondini, A. C., Cardinali, M., Fiorucci, F., Santangelo, M. and Chang, K. T.: Landslide inventory maps: New tools for an old problem, Earth-Science Rev., 112(1–2), 42–66, doi:10.1016/j.earscirev.2012.02.001, 2012.

Harp, E. L., Keefer, D. K., Sato, H. P. and Yagi, H.: Landslide inventories: The essential part of seismic landslide hazard analyses, Eng. Geol., 122(1–2), 9–21, doi:10.1016/j.enggeo.2010.06.013, 2011.

Huang, B., Zhao, B. and Song, Y.: Urban land-use mapping using a deep convolutional neural network with high spatial resolution multispectral remote sensing imagery, Remote Sens. Environ., 214(April), 73–86, doi:10.1016/j.rse.2018.04.050, 2018.

Hunt, K. M. R. and Menon, A.: The 2018 Kerala floods: a climate change perspective, Clim. Dyn., 54(3–4), 2433–2446, doi:10.1007/s00382-020-05123-7, 2020.

Karsli, F., Atasoy, M., Yalcin, A., Reis, S., Demir, O. and Gokceoglu, C.: Effects of land-use changes on landslides in a landslide-prone area (Ardesen, Rize, NE Turkey), Environ. Monit. Assess., 156(1–4), 241–255, doi:10.1007/s10661-008-0481-5, 2009.

Keyport, R. N., Oommen, T., Martha, T. R., Sajinkumar, K. S. and Gierke, J. S.: A comparative analysis of pixel- and object-based detection of landslides from very high-resolution images, Int. J. Appl. Earth Obs. Geoinf., 64(August 2017), 1–11, doi:10.1016/j.jag.2017.08.015, 2018.

https://doi.org/10.5194/essd-2020-83
Preprint. Discussion started: 29 June 2020

Kuriakose, S. L., Sankar, G. and Muraleedharan, C.: History of landslide susceptibility and a chorology of landslide-prone areas in the Western Ghats of Kerala, India, Environ. Geol., 57(7), 1553–1568, doi:10.1007/s00254-008-1431-9, 2009.

Lacroix, P., Zavala, B., Berthier, E. and Audin, L.: Supervised method of landslide inventory using panchromatic SPOT5 images and application to the earthquake-triggered landslides of Pisco (Peru, 2007, Mw8.0), Remote Sens., 5(6), 2590–2616, doi:10.3390/rs5062590, 2013.

Lahousse, T., Chang, K. T. and Lin, Y. H.: Landslide mapping with multi-scale object-based image analysis-a case study in the Baichi watershed, Taiwan, Nat. Hazards Earth Syst. Sci., 11(10), 2715–2726, doi:10.5194/nhess-11-2715-2011, 2011.

Lei, T., Xue, D., Lv, Z., Li, S., Zhang, Y. and Nandi, A. K.: Unsupervised change detection using fast fuzzy clustering for landslide mapping from very high-resolution images, Remote Sens., 10(9), 1–23, doi:10.3390/rs10091381, 2018.

Lei, T., Zhang, Q., Xue, D., Chen, T., Meng, H. and Nandi, A. K.: END-TO-END CHANGE DETECTION USING A SYMMETRIC FULLY CONVOLUTIONAL NETWORK FOR LANDSLIDE MAPPING School of Electronical and Information Engineering , Shaanxi University of Science and Technology , Institute of Geophysics and Geomatics , China University of, , 3027–3031, 2019.

Li, W. le, Huang, R. qiu, Tang, C., Xu, Q. and van Westen, C.: Co-seismic landslide inventory and susceptibility mapping in the 2008 Wenchuan earthquake disaster area, China, J. Mt. Sci., 10(3), 339–354, doi:10.1007/s11629-013-2471-5, 2013.

Li, Z., Shi, W., Myint, S. W., Lu, P. and Wang, Q.: Semi-automated landslide inventory mapping from bitemporal aerial photographs using change detection and level set method, Remote Sens. Environ., 175, 215–230, doi:10.1016/j.rse.2016.01.003, 2016.

Lu, P., Stumpf, A., Kerle, N. and Casagli, N.: Object-oriented change detection for landslide rapid mapping, IEEE Geosci. Remote Sens. Lett., 8(4), 701–705, doi:10.1109/LGRS.2010.2101045, 2011.

Lu, P., Qin, Y., Li, Z., Mondini, A. C. and Casagli, N.: Landslide mapping from multi-sensor data through improved change detection-based Markov random field, Remote Sens. Environ., 231(October 2018), 111235, doi:10.1016/j.rse.2019.111235, 2019.

Marcelino, E. V., Formaggio, A. R. and Maeda, E. E.: Landslide inventory using image fusion techniques in Brazil, Int. J. Appl. Earth Obs. Geoinf., 11(3), 181–191, doi:10.1016/j.jag.2009.01.003, 2009.

Martha, T. R., Kerle, N., Jetten, V., van Westen, C. J. and Kumar, K. V.: Characterising spectral, spatial and morphometric properties of landslides for semi-automatic detection using object-oriented methods, Geomorphology, 116(1–2), 24–36, doi:10.1016/j.geomorph.2009.10.004, 2010.

Martha, T. R., Kerle, N., Van Westen, C. J., Jetten, V. and Kumar, K. V.: Segment optimization and data-driven thresholding for knowledge-based landslide detection by object-based image analysis, IEEE Trans. Geosci. Remote Sens., 49(12 PART 1), 4928–4943, doi:10.1109/TGRS.2011.2151866, 2011.

Martha, T. R., Kerle, N., van Westen, C. J., Jetten, V. and Vinod Kumar, K.: Object-oriented analysis of multi-temporal panchromatic images for creation of historical landslide inventories, ISPRS J. Photogramm. Remote Sens., 67(1), 105–119, doi:10.1016/j.isprsjprs.2011.11.004, 2012.

https://doi.org/10.5194/essd-2020-83
Preprint. Discussion started: 29 June 2020

Martha, T. R., van Westen, C. J., Kerle, N., Jetten, V. and Vinod Kumar, K.: Landslide hazard and risk assessment using semi-automatically created landslide inventories, Geomorphology, 184, 139–150, doi:10.1016/j.geomorph.2012.12.001, 2013.

Martha, T. R., Kamala, P., Jose, J., Vinod Kumar, K. and Jai Sankar, G.: Identification of new Landslides from High Resolution Satellite Data Covering a Large Area Using Object-Based Change Detection Methods, J. Indian Soc. Remote Sens., 44(4), 515–524, doi:10.1007/s12524-015-0532-7, 2016.

Martha, T. R., Roy, P., Khanna, K., Mrinalni, K. and Vinod Kumar, K.: Landslides mapped using satellite data in the Western Ghats of India after excess rainfall during August 2018, Curr. Sci., 117(5), 804–812, doi:10.18520/cs/v117/i5/804-812, 2019.

Megha, V., Joshi, V., Kakde, N., Jaybhaye, A. and Dhoble, D.: Flood Mapping and Analysis using Sentinel Application Platform (SNAP) - A Case Study of Kerala, , 2(5), 486–488, 2019.

Miettinen, J., Gaveau, D. L. A. and Liew, S. C.: Comparison of visual and automated oil palm mapping in Borneo, Int. J. Remote Sens., 40(21), 8174–8185, doi:10.1080/01431161.2018.1479799, 2019.

Mishra, V., Aaadhar, S., Shah, H., Kumar, R., Pattanaik, D. R. and Tiwari, A. D.: The Kerala flood of 2018: combined impact of extreme rainfall and reservoir storage, Hydrol. Earth Syst. Sci. Discuss., (2017), 1–13, doi:10.5194/hess-2018-480, 2018.

Mohammady, M., Moradi, H. R., Zeinivand, H. and Temme, A. J. A. M.: A comparison of supervised, unsupervised and synthetic land use classification methods in the north of Iran, Int. J. Environ. Sci. Technol., 12(5), 1515–1526, doi:10.1007/s13762-014-0728-3, 2015.

Mohan Vamsee, A., Kamala, P., Martha, T. R., Vinod Kumar, K., Jai sankar, G. and Amminedu, E.: A Tool Assessing Optimal Multi-Scale Image Segmentation, J. Indian Soc. Remote Sens., 46(1), 31–41, doi:10.1007/s12524-017-0685-7, 2018.

Mondini, A. C., Guzzetti, F., Reichenbach, P., Rossi, M., Cardinali, M. and Ardizzone, F.: Semi-automatic recognition and mapping of rainfall induced shallow landslides using optical satellite images, Remote Sens. Environ., 115(7), 1743–1757, doi:10.1016/j.rse.2011.03.006, 2011.

Moosavi, V., Talebi, A. and Shirmohammadi, B.: Producing a landslide inventory map using pixel-based and object-oriented approaches optimized by Taguchi method, Geomorphology, 204, 646–656, doi:10.1016/j.geomorph.2013.09.012, 2014.

Oh, H. J. and Pradhan, B.: Application of a neuro-fuzzy model to landslide-susceptibility mapping for shallow landslides in a tropical hilly area, Comput. Geosci., 37(9), 1264–1276, doi:10.1016/j.cageo.2010.10.012, 2011.

Paul, S., Ghosh, S., Oglesby, R., Pathak, A., Chandrasekharan, A. and Ramsankaran, R.: Weakening of Indian Summer Monsoon Rainfall due to Changes in Land Use Land Cover, Sci. Rep., 6(December 2015), 1–10, doi:10.1038/srep32177, 2016.

Petley, D., Dunning, S. and Rosser, N. J.: The analysis of global landslide risk through the creation of a database of worldwide landslide fatalities, Landslide Risk Manag., 367–374, 2005.

Plank, S., Twele, A. and Martinis, S.: Landslide mapping in vegetated areas using change detection based on optical and polarimetric SAR data, Remote Sens., 8(4), doi:10.3390/rs8040307, 2016.

https://doi.org/10.5194/essd-2020-83
Preprint. Discussion started: 29 June 2020

Qin, Y., Lu, P. and Li, Z.: Landslide inventory mapping from Bitemporal 10 m Sentinel-2 images using change detection based markov random field, Int. Arch. Photogramm. Remote Sens. Spat. Inf. Sci. - ISPRS Arch., 42(3), 1447–1452, doi:10.5194/isprs-archives-XLII-3-1447-2018, 2018.

Rai, P., Choudhary, A. and Dimri, A. P.: Future precipitation extremes over India from the CORDEX-South Asia experiments, Theor. Appl. Climatol., 137(3–4), 2961–2975, doi:10.1007/s00704-019-02784-1, 2019.

Rai, P. K., Singh, G. P. and Dash, S. K.: Projected changes in extreme precipitation events over various subdivisions of India using RegCM4, Clim. Dyn., 54(1–2), 247–272, doi:10.1007/s00382-019-04997-6, 2020.

Reichenbach, P., Busca, C., Mondini, A. C. and Rossi, M.: The Influence of Land Use Change on Landslide Susceptibility Zonation: The Briga Catchment Test Site (Messina, Italy), Environ. Manage., 54(6), 1372–1384, doi:10.1007/s00267-014-0357-0, 2014.

Rosi, A., Tofani, V., Tanteri, L., Tacconi Stefanelli, C., Agostini, A., Catani, F. and Casagli, N.: The new landslide inventory of Tuscany (Italy) updated with PS-InSAR: geomorphological features and landslide distribution, Landslides, 15(1), 5–19, doi:10.1007/s10346-017-0861-4, 2018.

Sajinkumar, K. S. and Anbazhagan, S.: Geomorphic appraisal of landslides on the windward slope of Western Ghats, southern India, Nat. Hazards, 75(1), 953–973, doi:10.1007/s11069-014-1358-2, 2015.

Sajinkumar, K. S., Anbazhagan, S., Pradeepkumar, A. P. and Rani, V. R.: Weathering and landslide occurrences in parts of Western Ghats, Kerala, J. Geol. Soc. India, 78(3), 249–257, doi:10.1007/s12594-011-0089-1, 2011.

Samodra, G., Chen, G., Sartohadi, J. and Kasama, K.: Generating landslide inventory by participatory mapping: an example in Purwosari Area, Yogyakarta, Java, Geomorphology, 306, 306–313, doi:10.1016/j.geomorph.2015.07.035, 2018.

Sankar, G.: Monsoon Fury in Kerala — A Geo-environmental Appraisal, J. Geol. Soc. India, 92(4), 383–388, doi:10.1007/s12594-018-1031-6, 2018.

Santangelo, M., Marchesini, I., Bucci, F., Cardinali, M., Fiorucci, F. and Guzzetti, F.: An approach to reduce mapping errors in the production of landslide inventory maps, Nat. Hazards Earth Syst. Sci., 15(9), 2111–2126, doi:10.5194/nhess-15-2111-2015, 2015.

Seo, B., Bogner, C., Poppenborg, P., Martin, E., Hoffmeister, M., Jun, M., Koellner, T., Reineking, B., Shope, C. L. and Tenhunen, J.: Deriving a per-field land use and land cover map in an agricultural mosaic catchment, Earth Syst. Sci. Data, 6(2), 339–352, doi:10.5194/essd-6-339-2014, 2014.

Shashikanth, K., Ghosh, S., Vittal, H. and Karmakar, S.: Future projections of Indian summer monsoon rainfall extremes over India with statistical downscaling and its consistency with observed characteristics, Clim. Dyn., 51(1–2), 0, doi:10.1007/s00382-017-3604-2, 2018.

Singh, B., Singh, P., Supriya, K. and Singh, M.: An overview on Kerala floods : Loss of human lives as well as biodiversity in god ' s own Country An overview on Kerala floods : Loss of human lives as well as biodiversity in god ' s own Country, , (December), 0–3, doi:10.13140/RG.2.2.23925.22245, 2018.

https://doi.org/10.5194/essd-2020-83
Preprint. Discussion started: 29 June 2020

Solari, L., Del Soldato, M., Montalti, R., Bianchini, S., Raspini, F., Thuegaz, P., Bertolo, D., Tofani, V. and Casagli, N.: A Sentinel-1 based hot-spot analysis: landslide mapping in north-western Italy, Int. J. Remote Sens., 40(20), 7898–7921, doi:10.1080/01431161.2019.1607612, 2019.

Sreekumar, S.: Techniques for slope stability analysis: Site specific studies from Idukki district, Kerala, J. Geol. Soc. India, 73(6), 813–820, doi:10.1007/s12594-009-0065-1, 2009.

Srivastava, P. K., Han, D., Rico-Ramirez, M. A., Bray, M. and Islam, T.: Selection of classification techniques for land use/land cover change investigation, Adv. Sp. Res., 50(9), 1250–1265, doi:10.1016/j.asr.2012.06.032, 2012.

Stumpf, A. and Kerle, N.: Combining Random Forests and object-oriented analysis for landslide mapping from very high resolution imagery, Procedia Environ. Sci., 3, 123–129, doi:10.1016/j.proenv.2011.02.022, 2011.

Tasser, E., Mader, M. and Tappeiner, U.: Effects of land use in alpine grasslands on the probability of landslides, , 280, 271–280 [online] Available from: /Users/cibele/Documents/LITERATURE/ECOSYSTEM SERVICES/Tasser et al. 2003 - effects of lu chang in erosion - ALP.pdf, 2003.

Travelletti, J., Delacourt, C., Allemand, P., Malet, J. P., Schmittbuhl, J., Toussaint, R. and Bastard, M.: Correlation of multi-temporal ground-based optical images for landslide monitoring: Application, potential and limitations, ISPRS J. Photogramm. Remote Sens., 70, 39–55, doi:10.1016/j.isprsjprs.2012.03.007, 2012.

Trigila, A., Iadanza, C. and Spizzichino, D.: Quality assessment of the Italian Landslide Inventory using GIS processing, Landslides, 7(4), 455–470, doi:10.1007/s10346-010-0213-0, 2010.

Vasudevan, N. and Ramanathan, K.: Geological factors contributing to landslides: Case studies of a few landslides in different regions of India, IOP Conf. Ser. Earth Environ. Sci., 30(1), doi:10.1088/1755-1315/30/1/012011, 2016.

Vishnu, C. L., Sajinkumar, K. S., Oommen, T., Coffman, R. A., Thrivikramji, K. P., Rani, V. R. and Keerthy, S.: Satellite-based assessment of the August 2018 flood in parts of Kerala, India, Geomatics, Nat. Hazards Risk, 10(1), 758–767, doi:10.1080/19475705.2018.1543212, 2019.

van Westen, C.: Landslide inventory of the 2018 monsoon rainfall in Kerala, India, DANS, https://doi.org/10.17026/dans-x6c-y7x2, 2020.

van Westen, C. J., Castellanos, E. and Kuriakose, S. L.: Spatial data for landslide susceptibility, hazard, and vulnerability assessment: An overview, Eng. Geol., 102(3–4), 112–131, doi:10.1016/j.enggeo.2008.03.010, 2008.

Van Westen, C.: Remote sensing for natural disaster management, Int. Arch. Photogramm. Remote Sens. Spat. Inf. Sci. - ISPRS Arch., 33, 1609–1617, 2000.

Xu, C.: Preparation of earthquake-triggered landslide inventory maps using remote sensing and GIS technologies: Principles and case studies, Geosci. Front., 6(6), 825–836, doi:10.1016/j.gsf.2014.03.004, 2015.

Xu, C., Xu, X., Dai, F., Wu, Z., He, H., Shi, F., Wu, X. and Xu, S.: Application of an incomplete landslide inventory, logistic regression model and its validation for landslide susceptibility mapping related to the May 12, 2008 Wenchuan earthquake of China, Nat. Hazards, 68(2), 883–900, doi:10.1007/s11069-013-0661-7, 2013.

https://doi.org/10.5194/essd-2020-83
Preprint. Discussion started: 29 June 2020

Yang, X. and Chen, L.: Using multi-temporal remote sensor imagery to detect earthquake-triggered landslides, Int. J. Appl. Earth Obs. Geoinf., 12(6), 487–495, doi:10.1016/j.jag.2010.05.006, 2010.

Yu, B. and Chen, F.: A new technique for landslide mapping from a large-scale remote sensed image: A case study of Central Nepal, Comput. Geosci., 100(August 2016), 115–124, doi:10.1016/j.cageo.2016.12.007, 2017.

Zhong, C., Liu, Y., Gao, P., Chen, W., Li, H., Hou, Y., Nuremanguli, T. and Ma, H.: Landslide mapping with remote sensing: challenges and opportunities, Int. J. Remote Sens., 00(00), 1–27, doi:10.1080/01431161.2019.1672904, 2019.

Table 1: The number of landslides per district in Kerala for the various data sources

District \ Source	NRSC	GSI	GSI+NRSC	New	Total /%
Idukki	607	685	256	675	2223/47.02
Pathanamthitta	66	24	7	9	106/2.24
Kottayam	43	18	13	2	76/1.61
Thrissur	206	33	17		256/5.41
Ernakulam	94	10	3		107/2.26
Palakkad	649	54	36	54	793/16.77
Kozhikode	97	23	18	90	228/4.82
Malappuram	312	59	36	22	429/9.07
Wayanad	250	53	26	2	331/7.00
Kannur	116	14	10	1	141/3.00
Kasaragod	24				24/0.51
Kollam	10				10/0.21
Thiruvananthapuram	3			1	4/0.09
Total	2477	973	422	856	4728

Table 2: The number of landslide classified by types in each district in Kerala

District \ Type	Surficial Slide (SS)	Debris Flow (DF)	Rockfall (RF)
Idukki	1421	679	123
Pathanamthitta	13	92	1
Kottayam	11	65	
Thrissur	20	234	2
Ernakulam	11	96	
Palakkad	92	699	2
Kozhikode	18	204	6

https://doi.org/10.5194/essd-2020-83
Preprint. Discussion started: 29 June 2020

Malappuram	66	358	5
Wayanad	68	252	11
Kannur	19	120	2
Kasaragod	19	5	
Kollam	1	9	
Thiruvananthapuram	1	3	
Total	1760	2816	152

https://doi.org/10.5194/essd-2020-83
Preprint. Discussion started: 29 June 2020

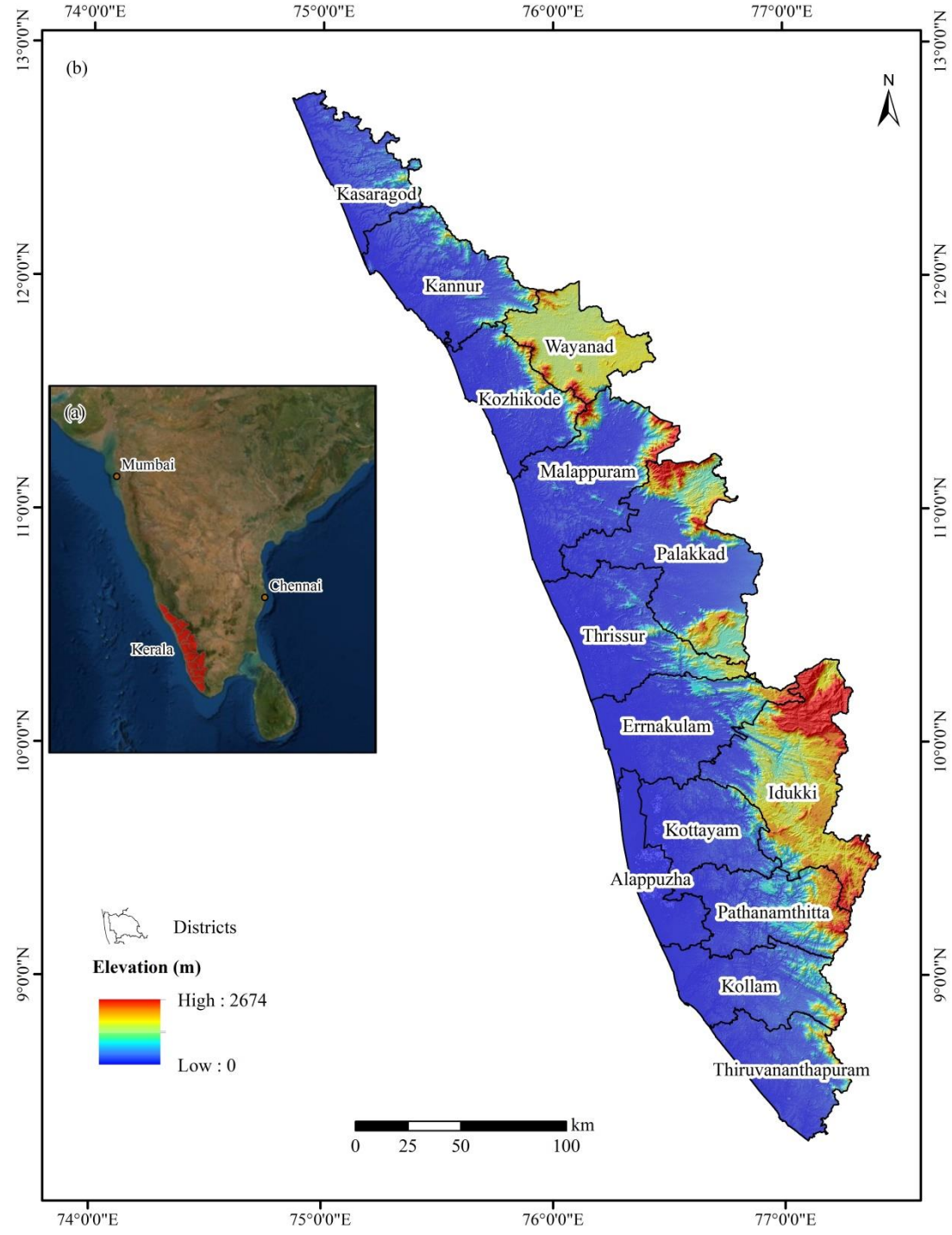

560 **Figure 1: Overview map of Kerala with districts and elevation.**

https://doi.org/10.5194/essd-2020-83
Preprint. Discussion started: 29 June 2020

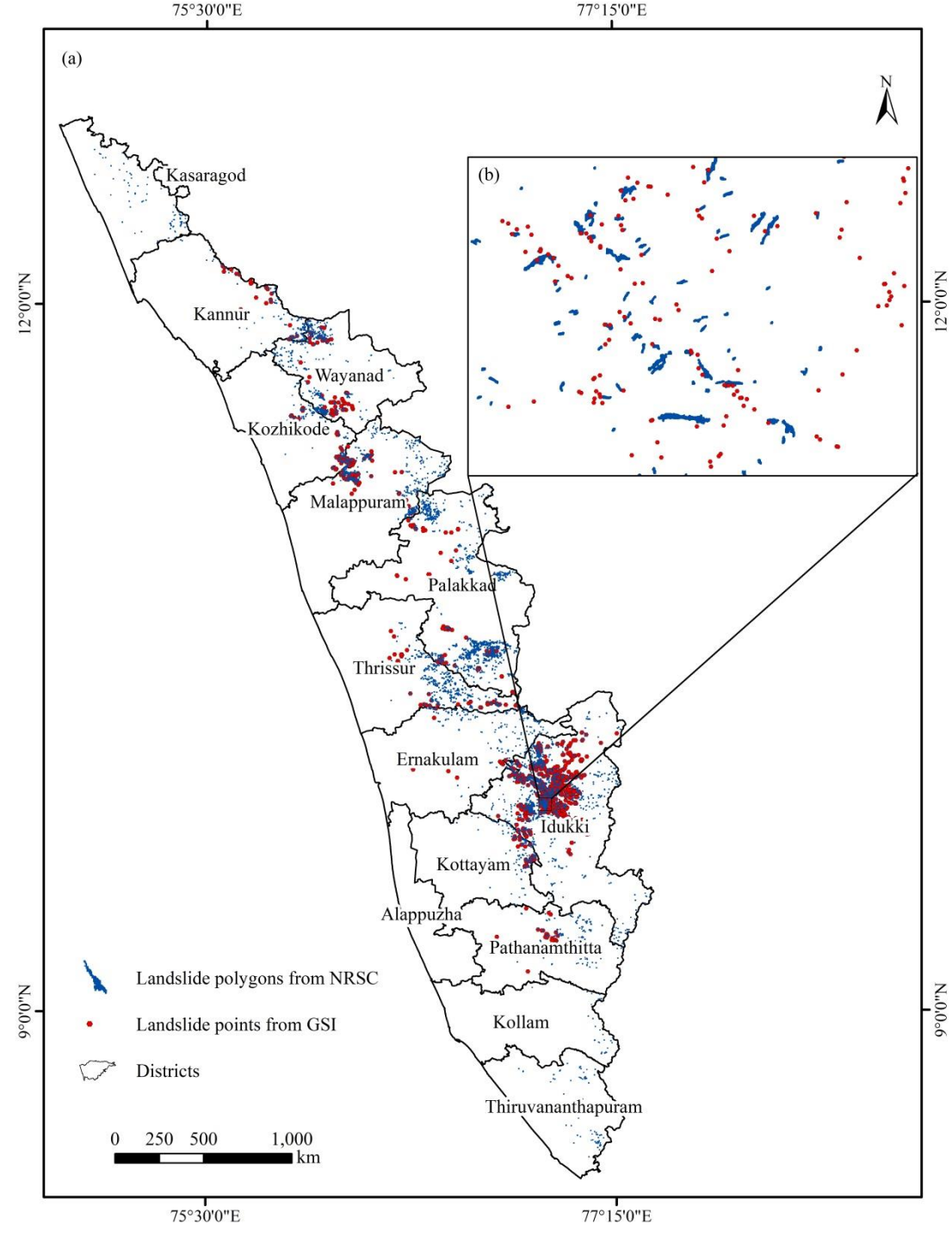

Figure 2: Overview map of the existing inventories.

https://doi.org/10.5194/essd-2020-83
Preprint. Discussion started: 29 June 2020

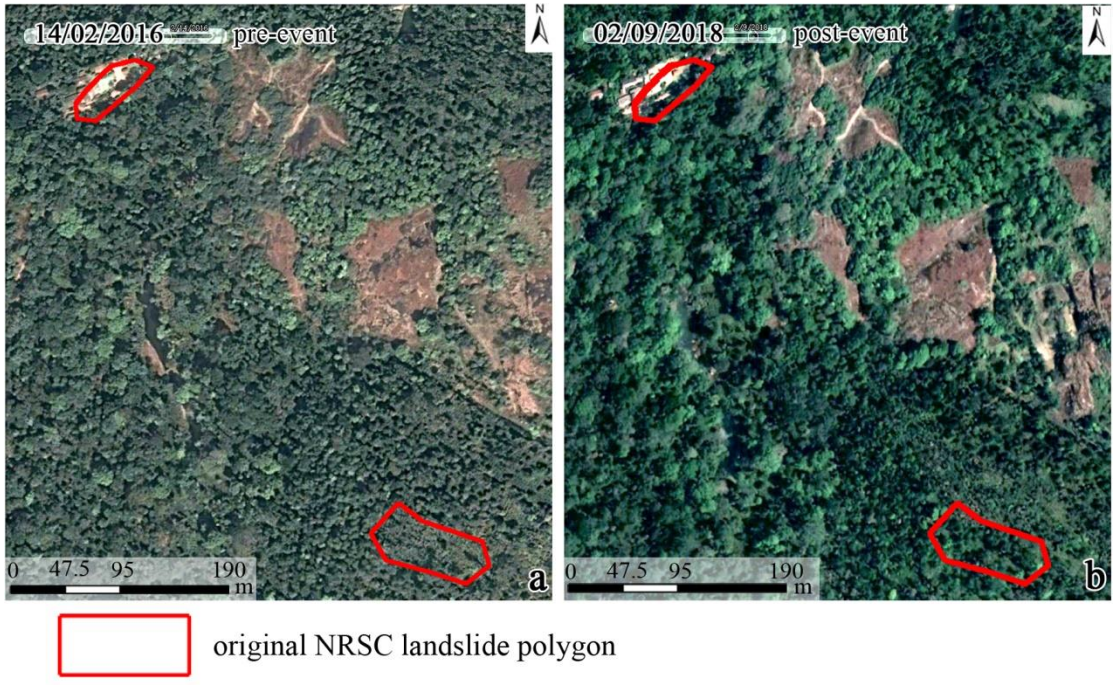

Figure 3: Examples of landslides in the NRSC inventory that were not considered as actual landslides after visual inspection. The examples in a and b show that there are no visible scarps before and after the event near the marked polygons. Basemap data© 2019 Google

https://doi.org/10.5194/essd-2020-83
Preprint. Discussion started: 29 June 2020

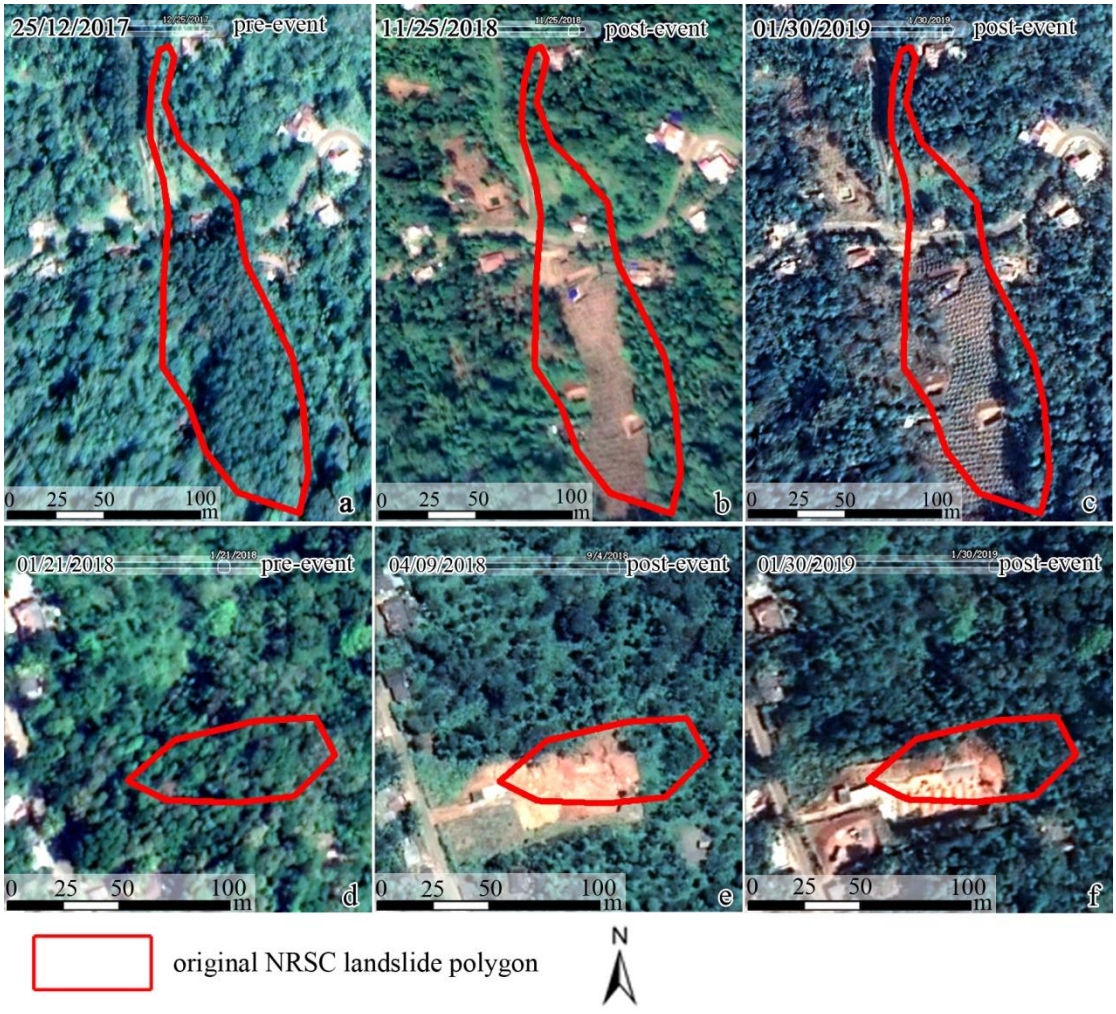

Figure 4: Examples of landslides in the NRSC inventory that were not considered as actual landslides after visual inspection. The example in a, b, and c shows that the changes in the polygon before and after the event were caused by vegetation clearing, and agricultural activities. Images d, e, and f show that the changes near the polygon before and after the event were caused by building construction. Basemap data© 2019 Google

https://doi.org/10.5194/essd-2020-83
Preprint. Discussion started: 29 June 2020

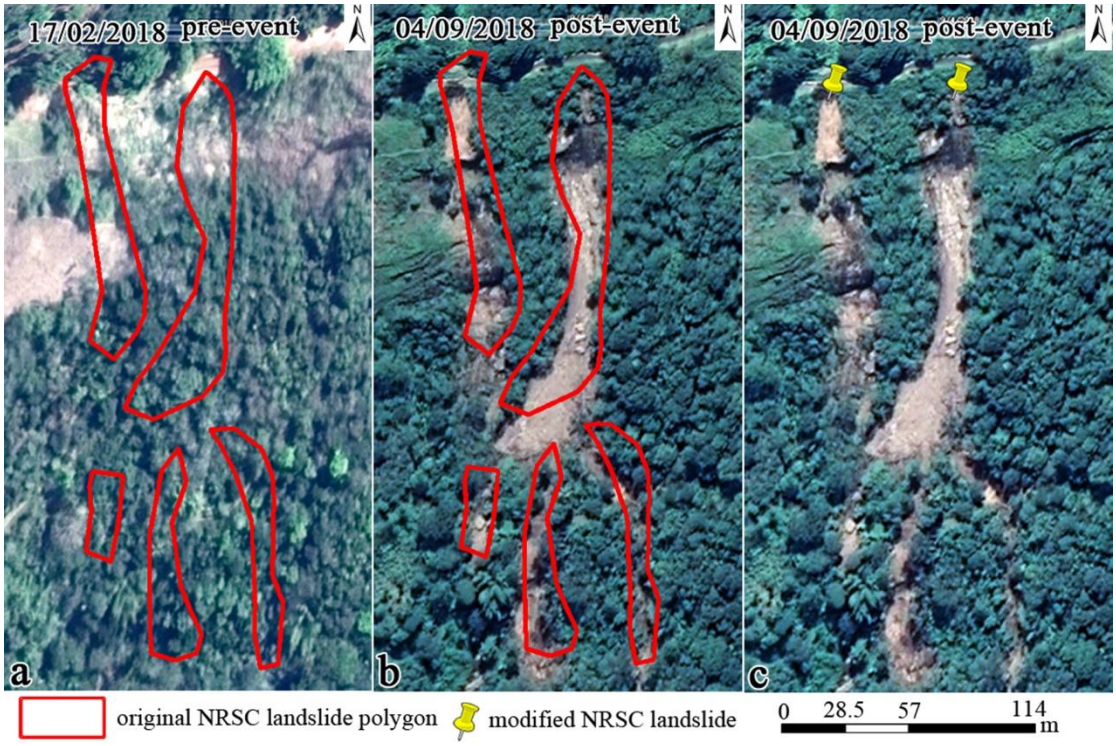

Figure 5: Example of the original NRSC landslide polygons which were combined and converted into points and digitized on the top of the scarps- (a) pre-landslide image; (b) post-landslide image; (c) creation of a new inventory using points. Basemap data© 2019 Google

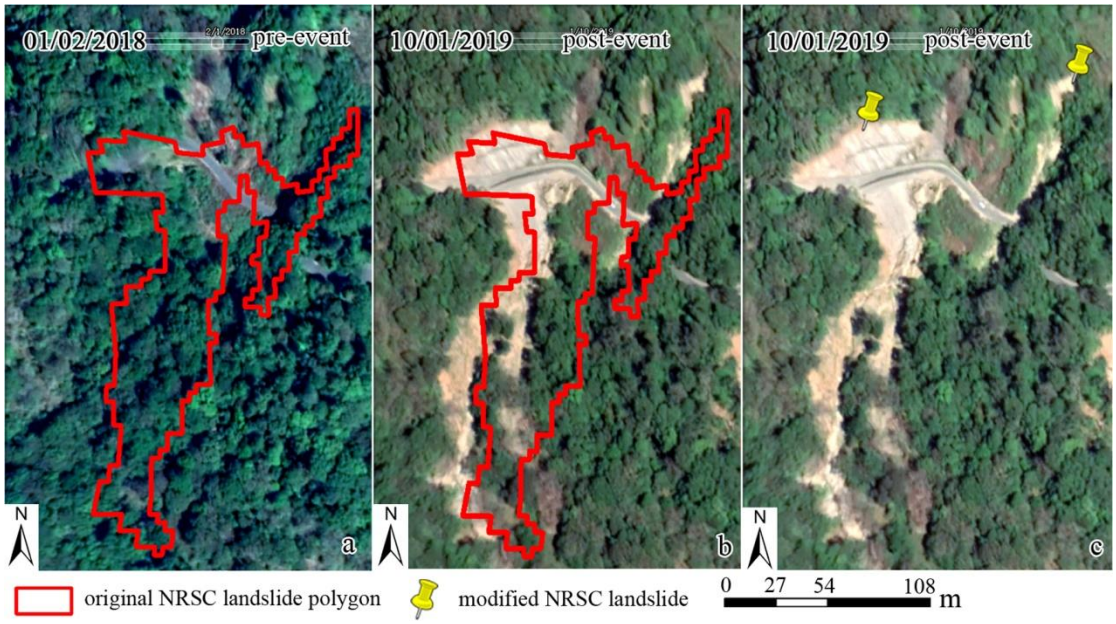

https://doi.org/10.5194/essd-2020-83
Preprint. Discussion started: 29 June 2020

Open Access Earth System Science Data Discussions

Figure 6: Example of an original NRSC landslide polygon which was separated and converted into several landslides, marked by points and digitized on the top of the scarps. (a) pre-landslide image; (b) post-landslide image; (c) creation of a new inventory using points. Basemap data© 2019 Google

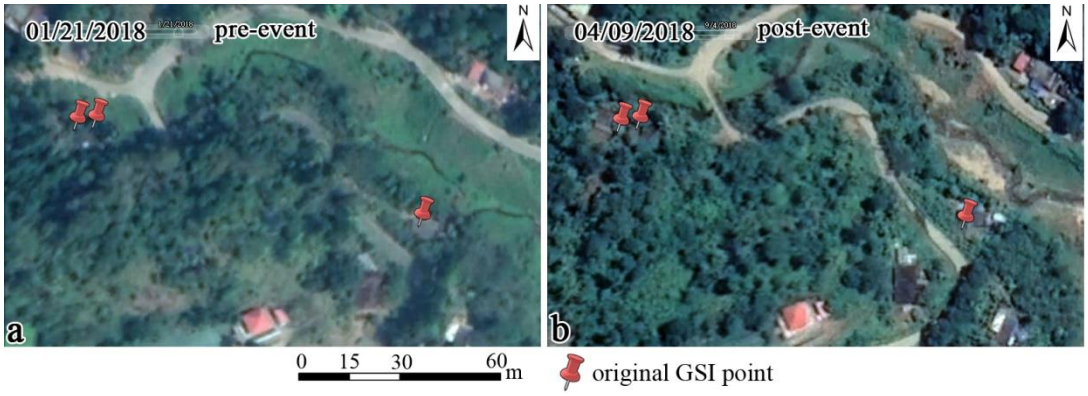

Figure 7: Example of the original GSI landslide points that were accepted even if no manifestation of landslide scarps was visible in pre- and post- event images within Google Earth. We assumed that landslide were properly marked in the field by the surveyors, and that they must have been very small and hidden from view by surrounding vegetation. Basemap data© 2019 Google

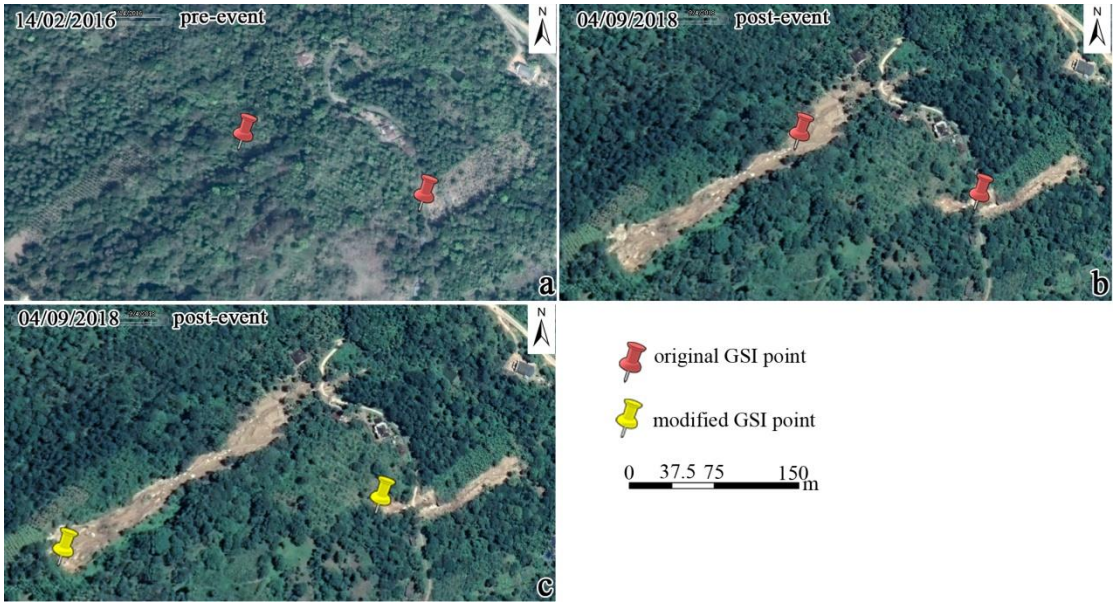

Figure 8: Example of the original GSI landslide points that were shifted to the top of the landslide scarps. Basemap data© 2019 Google

https://doi.org/10.5194/essd-2020-83
Preprint. Discussion started: 29 June 2020

590

Figure 9: Example of vegetation re-growth sheltering the scarps on Google Earth images due to the large time gap between the event and the first available images within Google Earth. The original NRSC landslide polygons were converted into points and digitized on the top of the scarps at NRSC based on Resourcesat-2 LISS-IV images ((a) pre-landslide image; (b) post-landslide image; (c) creation of a new inventory using points). Basemap data© 2019 Google

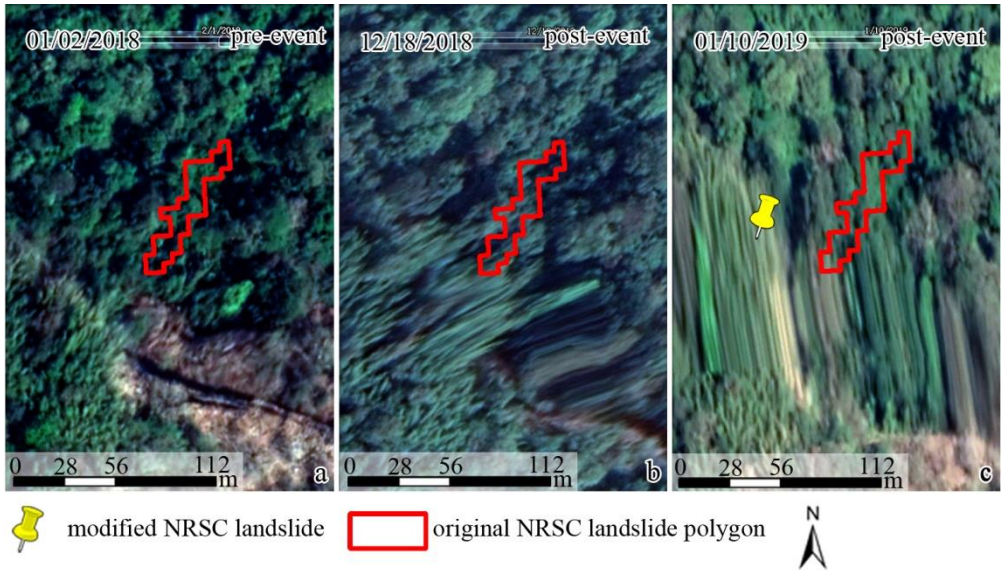

595

Figure 10: Example of distorted images in Google Earth where it was not possible to check the original NRSC landslide polygons. They were converted into points and digitized on the top of the scarps based on Resourcesat-2 LISS-IV images ((a) pre-landslide image; (b) post-landslide image; (c) creation of a new inventory using points based on post-landslide). Basemap data© 2019 Google

https://doi.org/10.5194/essd-2020-83
Preprint. Discussion started: 29 June 2020

Figure 11: Example of the presence of darks shadows in the post-event images in Google Earth images, making it impossible to check the original NRSC landslide polygons. Basemap data© 2019 Google

Figure 12: Example of the obstruction of view by clouds where the original NRSC landslide polygons could not be checked. Basemap data© 2019 Google

https://doi.org/10.5194/essd-2020-83
Preprint. Discussion started: 29 June 2020

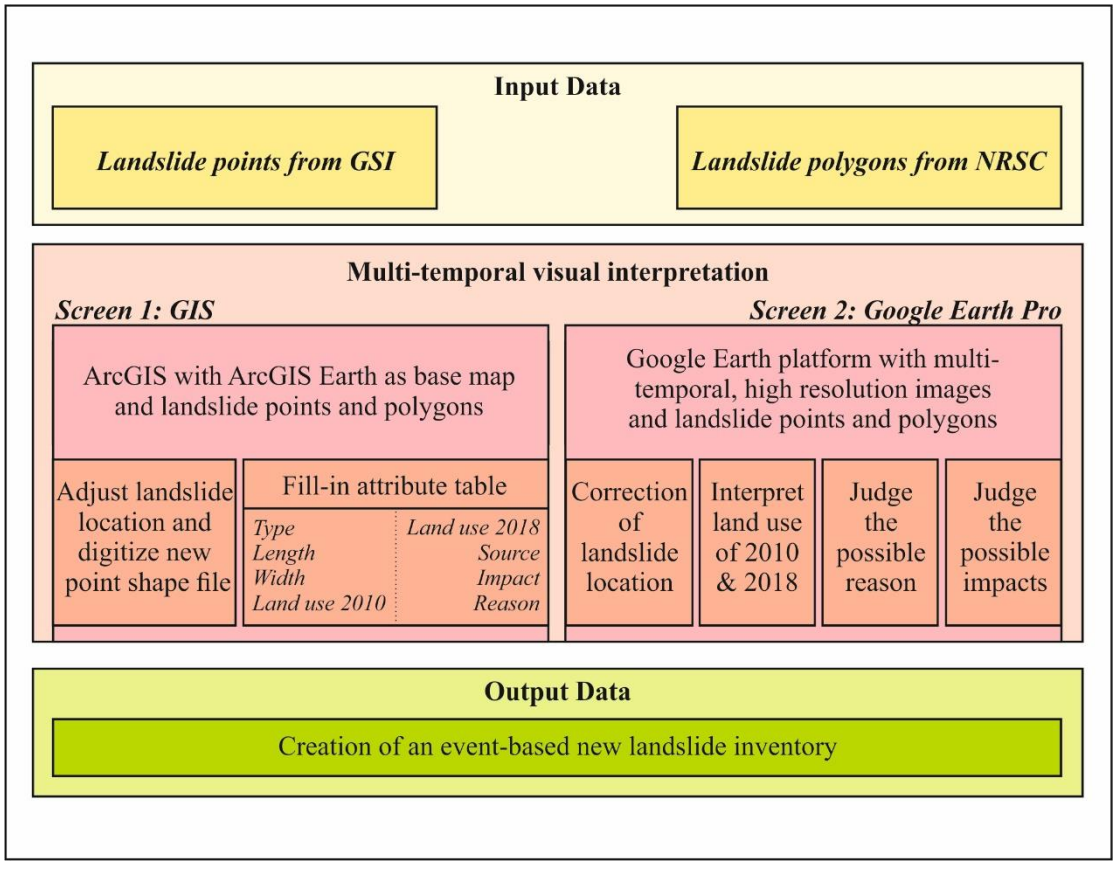

Figure 13: Overview of the methodology adopted for the creation of a new landslide inventory in this study.

https://doi.org/10.5194/essd-2020-83
Preprint. Discussion started: 29 June 2020

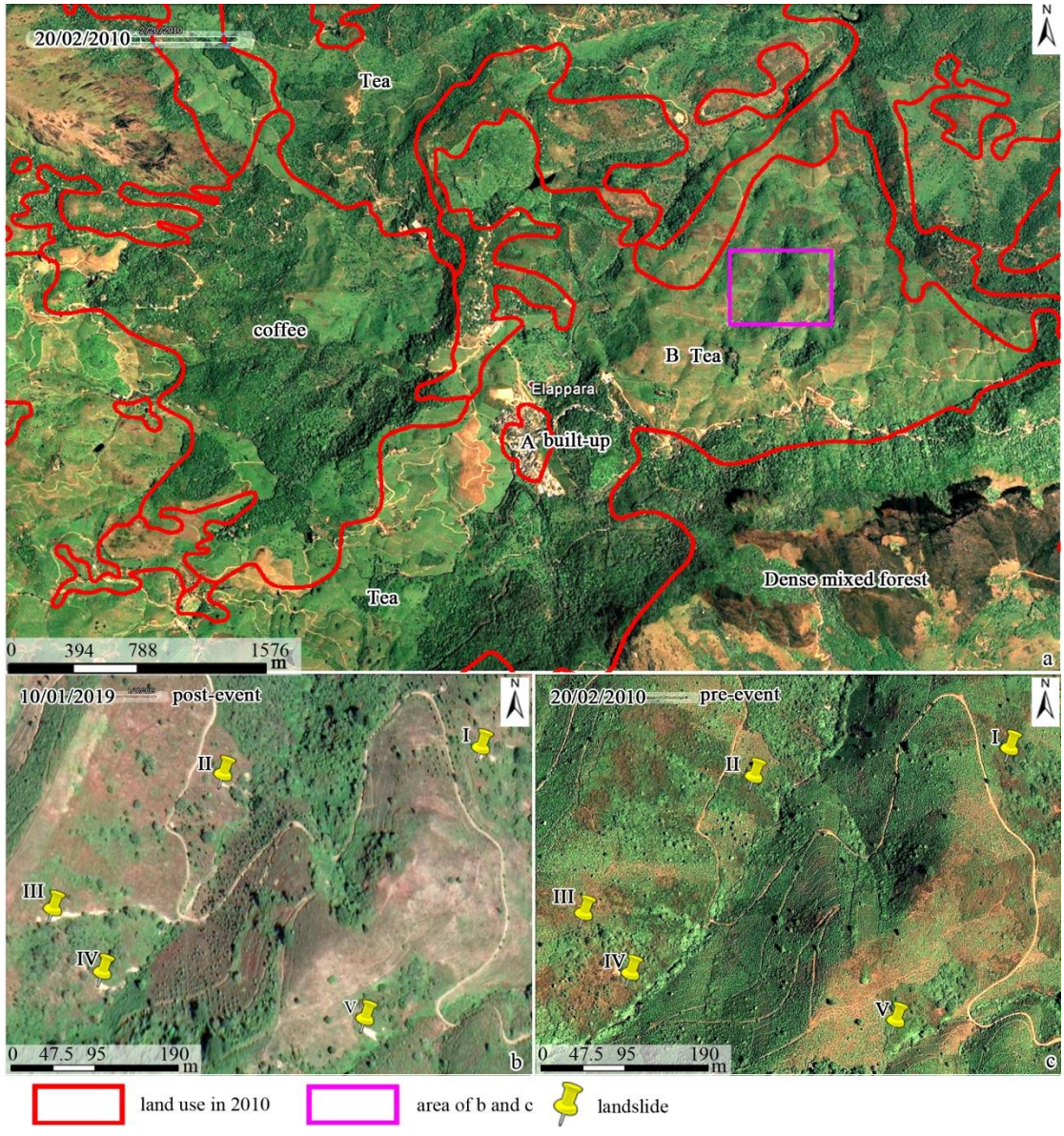

Figure 14: Example of the problem in using the available land use map. The boundaries of the available 1:50,000 land use map from 2010 is shown on a high resolution image of the same year. The detailed images shown in b and c contains many more land use types, than the single one indicated in the map, leading to wrong correlations between landslides and land use. Basemap data© 2019 Google

https://doi.org/10.5194/essd-2020-83
Preprint. Discussion started: 29 June 2020

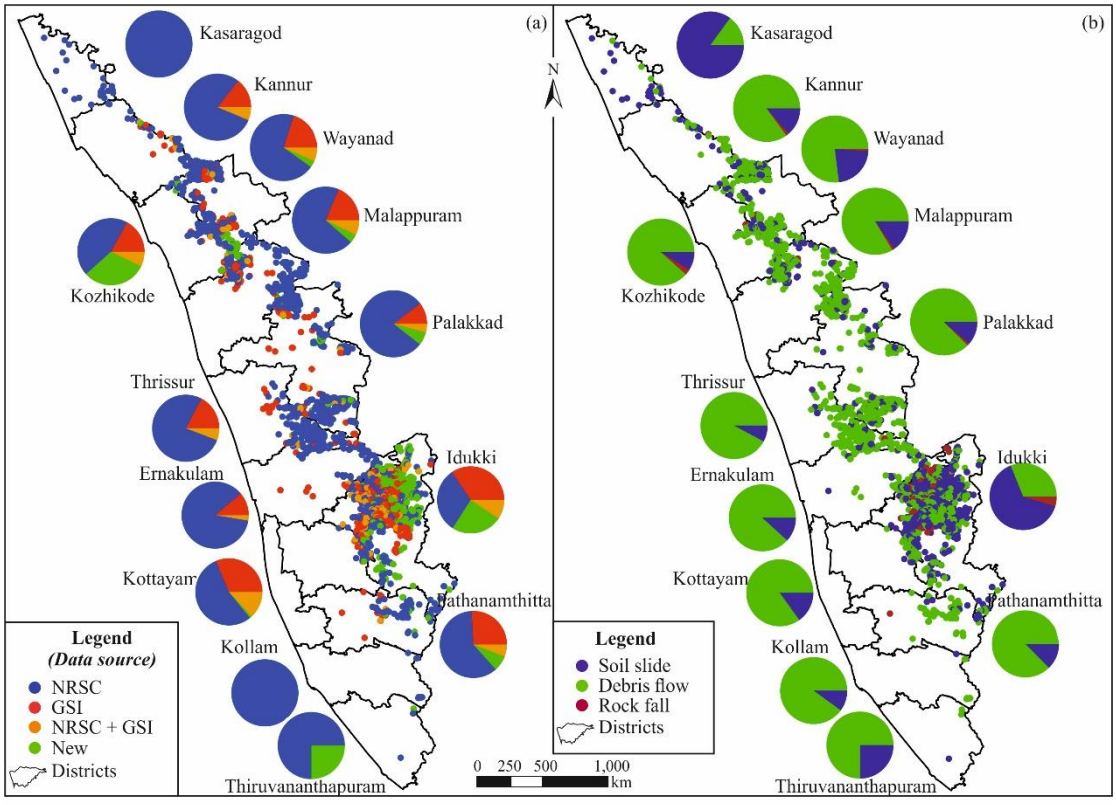

Figure 15: Map of the final landslide inventory dataset (a. distribution according to the source of the data, b. distribution of different landslide types).

https://doi.org/10.5194/essd-2020-83
Preprint. Discussion started: 29 June 2020

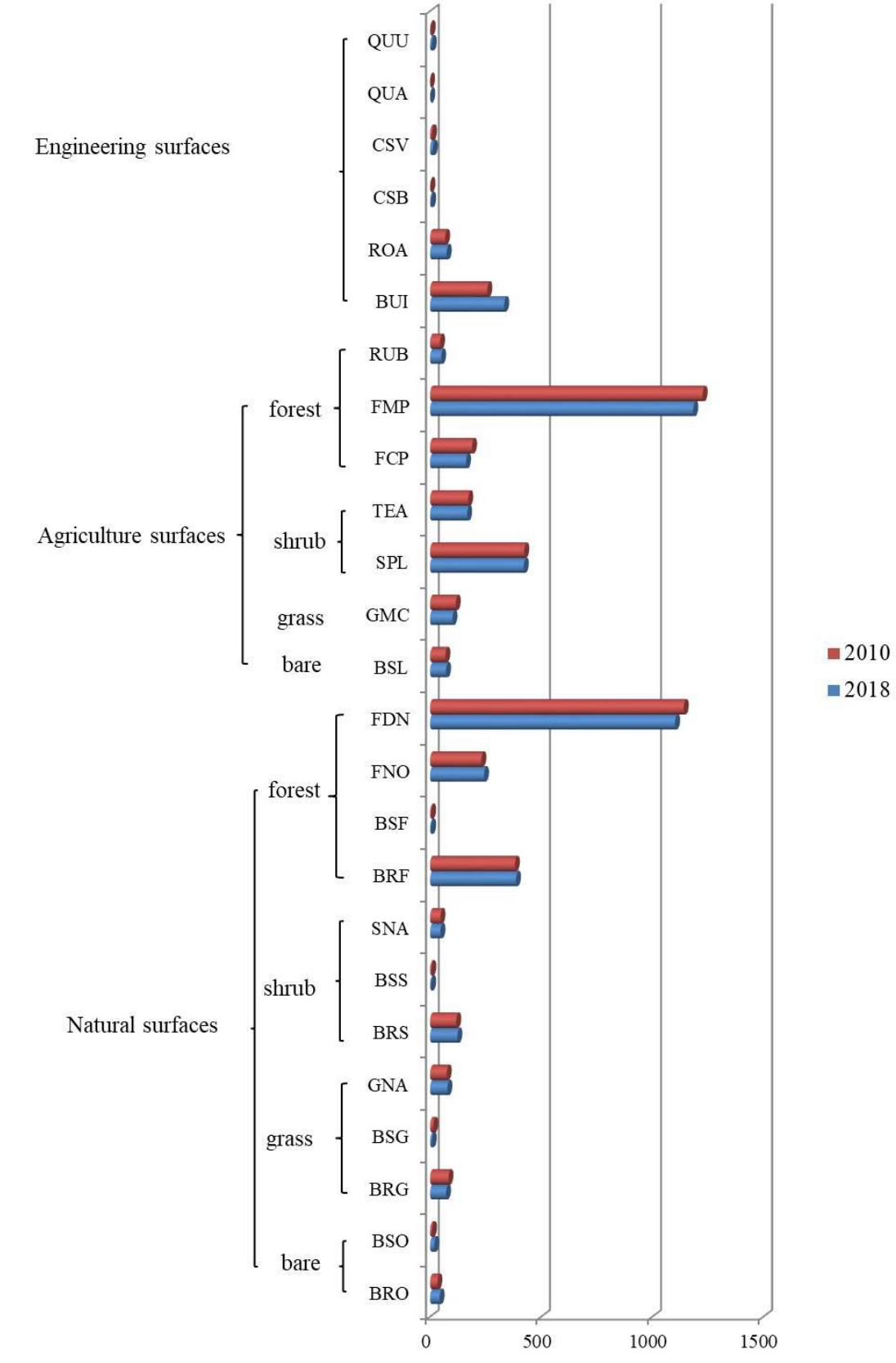

https://doi.org/10.5194/essd-2020-83
Preprint. Discussion started: 29 June 2020

Open Access Earth System Science Data Discussions

Figure 16: General land use types of all landslides in Kerala (QUU-quarry in use, QUA-quarry abandoned, CSV-vegetated cut slopes, CSB-bare cut slopes, ROA-roads, BUI-buildings, RUB-rubber plantation, FMP- mixed forest plantation, FCP-forest plantation, TEA-tea plantation, SPL-shrub plantation, GMC-meadows (refers to cultivated grassland), BSL-bare farmland, FDN-dense natural forest, FNO-open natural forest, BSF- bare soil with isolated forests, BRF-bare rock with isolated forests, SNA-natural shrub land, BSS-bare soil with isolated shrubs, BRS-bare rock with isolated shrubs, GNA-natural grass land, BSG-bare soil with isolated grass, BRG-bare rock with isolated grass, BSO-bare soil, BRO-bare rock)

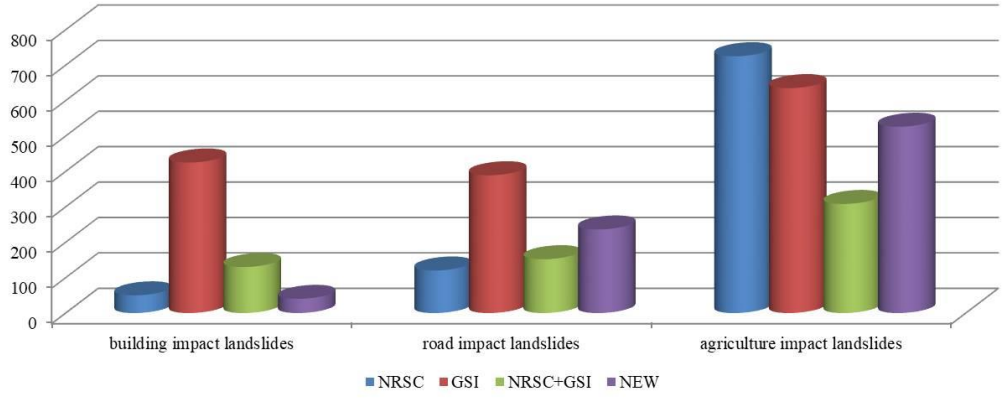

Figure 17:Damaging landslides of different source.

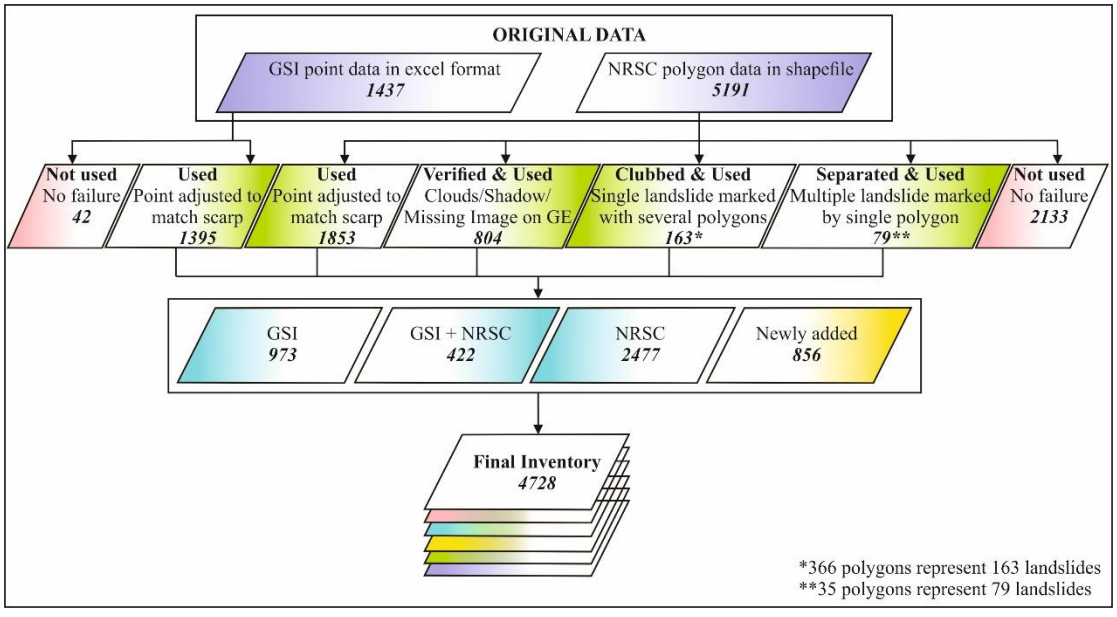

Figure 18: Overview of the procedure to generate the complete landslide inventory with the number of landslides indicated.